Breast Cancer Research and Treatment (2019) 177:419–426
https://doi.org/10.1007/s10549-019-05297-7

CLINICAL TRIAL

Preliminary results of computer-aided diagnosis for magnetic resonance imaging of solid breast lesions

Qiujie Yu[1] · Kuan Huang[2] · Ye Zhu[3] · Xiaodan Chen[4] · Wei Meng[1]

Received: 18 February 2019 / Accepted: 25 May 2019 / Published online: 15 June 2019

Abstract

Purpose The present study aimed to determine suitable optimal classifiers and investigate the general applicability of computer-aided diagnosis (CAD) to compare magnetic resonance (MR)-CAD with MR imaging (MRI) in distinguishing benign from malignant solid breast masses.

Methods We analyzed a total of 251 patients (mean age: 44.8 ± 12.3 years; range: 21–81 years) with 274 breast masses (154 benign masses, 120 malignant masses) using a Gaussian mixture model and a random forest machine model for segmentation and classification.

Results The diagnostic performance of MRI alone and MRI plus CAD were compared with respect to sensitivity, specificity, and area under the curve (AUC), using receiver operating characteristic curve analysis. The discriminating power to detect malignancy using MR-CAD with an AUC of 0.955 (sensitivity was 95.8% and the specificity was 92.9%) was significantly higher than that of MRI alone with an AUC of 0.785 (sensitivity was 71.7% and the specificity was 85.7%).

Conclusion CAD is feasible to differentiate breast lesions, and it can complement MRI, thereby making it easier to diagnose breast lesions and obviating the need for unnecessary biopsies.

Keywords Breast lesions · MRI · Computer-aided diagnosis · Gaussian mixture · Random forest

Introduction

To screen for breast cancer in women at high risk for developing the disease, ultrasonography and mammography are the first two recommended methods, while magnetic resonance imaging (MRI) is increasingly being used because it has higher sensitivity than that two methods [1–3]. MRI is especially helpful in young women with dense breast tissue when a palpable mass is not visualized on a mammogram [4] and it can depict small, early-stage malignancies of dense breasts [5, 6]. Issues such as imaging quality and human error have increased the misdiagnosis of breast cancer during radiologists' interpretation. With the development of computer applications, many imaging tools based on computer-aided diagnosis (CAD) technologies have been developed to enhance diagnostic accuracy. CAD also has the potential to improve observer reproducibility in dynamic contrast material-enhanced MR imaging [7–9]. From segmentation to classification, CAD comprises many methods. The Gaussian mixture model is one kind of segmentation method and is used in many domains. Chaddad [10] used a Gaussian mixture model to realize the segmentation of brain

✉ Wei Meng
articlemengwei@163.com

Qiujie Yu
yuqiujie2011@sina.com

Kuan Huang
hk57816631@gmail.com

Ye Zhu
akiko1991@126.com

Xiaodan Chen
xiaodanchen@qq.com

1 Radiology Department, Harbin Medical University, The Third Affiliated Hospital of Harbin Medical University, 150 Haping Road, Harbin 150081, Heilongjiang, China

2 Department of Computer Science, Utah State University, Old Main Hill, Logan, Utah 84322, USA

3 Department of Obstetrics and Gynecology, Peking University People's Hospital, No.11 Xizhimen South Street, Xicheng District, Beijing 100044, China

4 Department of Computer Technology, Harbin Institute of Technology University, 92 West street, Harbin 150000, Heilongjiang, China

MRI. However, there are relatively few studies on the use of the Gaussian mixture model in breast MRI. A pilot study by Banaie [11] showed that random forest (rf) has the discriminative power to effectively differentiate between benign and malignant mass lesions. Some CAD schemes were developed to help identify potentially malignant regions in breast dynamic contrast-enhanced MRI (DCE-MRI) and to bring them to the attention of radiologists. Gallego-Ortiz [12] extracted image data from DCE-MRI and analyzed them using feature selection techniques and binary, multiclass, and cascade classifiers. Finally, the separately optimized feature selection and training classifiers for mass and non-mass lesions improved the accuracy of CAD for breast MRI. Gubern-Merida [13] used blob and relative enhancement of voxel features to locate the lesion and then corrected the motion artifacts and segment of the breast. However, most research has focused only on the CAD systems, ignoring the combination of clinical experiences of radiologists. The purpose of the present study was to determine suitable optimal classifiers and investigate the general applicability of CAD to compare MR-CAD with MR imaging to distinguish benign from malignant solid breast masses.

Materials and methods

Breast MR imaging data sets

The study was a retrospective study and the protocol was approved by the Institutional Ethics Committee of our University for human research. Informed consent was obtained from all the patients. Breast MR imaging studies were selected from our Pacs room, which links clinical information with radiological and pathological reports to MR images. From April 2015 to December 2017, a total of 251 patients (mean age: 44.8 ± 12.3 years; range: 21–81 years) with 274 masses (mean size 27.8 ± 16.3 mm, range 8–63 mm) who underwent core-needle biopsy or surgery were included in our study. Five patients were excluded from the study group because the pathological results were lacking or imprecise.

MR images were obtained using a 3.0T MR scanner (Philips Achieva 3.0T). The patients adopted a prone position and put their breasts into the dedicated phased array breast coil. Imaging parameters for DCE-MRI were are as follows:

Axial T1-weighted imaging (repetition time (TR) = 495 ms; echo time (TE) = 10 ms; slice thickness/gap = 3 mm/0 mm; matrix = 512; number of signal averaged (NSA) = 1; field of view (FOV) = 340 mm × 340 mm); axial T2-weighted imaging (TR = 4213 ms, TE = 120 ms, slice thickness/gap = 3 mm/0 mm, matrix = 512, NSA = 1, FOV = 340 mm × 340 mm); T2-weighted fat-saturated imaging using a spectral selection attenuated inversion recovery (SPAIR) (TR = 4216 ms, TE = 60 ms, inversion delay (IR) = 120 ms, slice thickness/gap = 3 mm/0 mm, matrix = 352, NSA = 1, FOV = 340 mm × 340 mm); and T1-weighted high-resolution isotropic volume examination (THRIVE) (TR = 4.4 ms, TE = 2.2 ms, flip angle = 12°; matrix = 352; FOV = 340 mm × 340 mm; number of sections = 110; acquisition time: 256 s). MR imaging data sets were acquired once before gadolinium (Gd)-diethylenetriamine penta-acetic acid (DTPA) (Bayer scheming pharma AG, Berlin, Germany) injection and at 90 s intervals upon injection of 0.1 mmol/kg Gd-DTPA (followed by an intravenous saline flush of 20 ml), for a total imaging duration of 5–8 min.

Tumor segmentation

We chose the first sequence of DCE-MRI for segmentation and feature extraction. The contrast of the image was enhanced by normalizing the histogram of the original image. The normalized images were divided into blocks, and each block was marked as breast area and non-breast area using the SVM method. The MR images are separated into 50 × 50 pixel non-overlapping patches. The gray level and co-occurrence matrix features of each patch of the image were extracted and these features were used to train an SVM classifier. Each patch was classified as either a normal area or a tumor area. Finally, the classifier was used to find the region of interest (ROI) of the breast cancer. The gray level co-occurrence matrix was used as the feature of the ROI. It describes the texture characteristics of the images. The statistical analysis of the spatial correlation and the use of a variety of texture descriptors overwrote the gray level of the relevant pixels, so that the texture features could be clearly revealed. The gray level co-occurrence matrix describes the image features as follows: Contrast, energy, entropy, and correlation. We used the gray level co-occurrence matrix to extract the gray scale features of each 10 × 10 small area in the image. In this experiment, the local texture features of each pixel were extracted from the 10 × 10 patch around the pixel. Features were extracted from co-occurrence matrix: Entropy and reciprocal difference. Each feature was extracted at three different relative distances (D = 1, 2, and 3), and four different relative angles (0, 45, 90, and 135 degrees). To reduce the dimension of a feature, the average values of the feature in four different degrees were calculated. Thus, there were 3 × 2 = 6 texture features. Then, the mean value and variance of the gray-level intensity of the 10 × 10 patch were also used, resulting in an 8-dimension feature being used for segmentation. The extracted features of the breast part were input into a Gaussian mixture model (GMM) to construct the model for background and tumors. GMM is a commonly used model to describe the distribution

of mixed density functions. It uses the weighted sum of several Gaussian probability density functions to describe the distribution of vector features in the probability space. The expectation–maximization (EM) algorithm was used to estimate the three parameters (mixture coefficient, mean values, and covariances) of the GMM models. The EM algorithm can be separated into the E step and the M step, in which the E step uses the initial parameters value to calculate the posterior probability, and then the M step uses the maximum likelihood estimation and the posterior probability to calculate the new values of the three parameters. In this experiment, all images were fused into a huge matrix to obtain the posterior probability and then the posterior probability was maximized to obtain new parameters. The calculation formula of posterior probability is shown below:

$$w_j^{(i)} = p\left(z^{(i)} = j | x^{(i)}; \phi, \mu, \sum\right).$$

The calculation formulas of gaussian parameters are as follows:

$$\phi_j = \frac{1}{m}\sum_{i=1}^{m} w_j^{(j)}; \mu_j = \frac{\sum_{i=1}^{m} w_j^{(i)} x^{(i)}}{\sum_{i=1}^{m} w_j^{(i)}}; \sum_j = \frac{\sum_{i=1}^{m} w_j^{(i)} \left(x^{(i)} - \mu_j\right)\left(x^{(i)} - \mu_j\right)^T}{\sum_{i=1}^{m} w_j^{(i)}}.$$

X is the grayscale value of pixels and m is the number of pixels. Before using the algorithm to train the model, the parameters must be initialized. Using different initialization methods will affect the iteration speed of the algorithm. GMM commonly uses initialization methods, such as random initialization, and the average method, which uses the prior knowledge of the sample distribution, in which the latter is better than the former. In this study, the model parameters were initialized using the 3-mean clustering model, and the parameters and likelihood functions were constantly updated using the EM algorithm. Iteration was terminated when the difference of the likelihood between the two times was less than 1e-5. Three Gaussian models were established for the background and tumor of the image using the obtained Gaussian parameters. Tumor and background were divided according to the maximum probability.

Tumor feature extraction and selection

Based on normalized Gray-Gradient Co-occurrence Matrix (GGCM), a series of quadratic statistical features could be calculated. The following are 15 commonly used digital features: Small gradient advantage, large gradient advantage, grayscale distribution inhomogeneity, gradient distribution inhomogeneity, energy, average gray level, gradient, gray mean–variance, gradient mean–variance, gradient entropy, correlation, gray entropy, entropy of mixing, inertia, and homogeneity. In this experiment, the GGCM and the gray-level co-occurrence matrix (GLCM) were used to extract the above 51 gray scale features (mean, variance, entropy and in the case of step sizes of 1, 2, and 3, respectively, and the direction is 0, 45, 90 and 135, respectively, the characteristics of contrast, correlation, energy, and homogeneity) and the 15 gradient features. The principal component analysis (PCA) computes a set of new and linearly independent variables known as principal components (PCs). PCs account for most of the variance of the original variables. Extract the 13 shape characteristics of the image in the tumor: roundness, aspect ratio, average normalized radial length, normalized radial length standard deviation, entropy of the average normalized radial length, area ratio, aspect ratio, number of lobular, needle shape, boundary roughness, direction Angle, normalization of ellipse pupil ellipse normalized contour. In this experiment, the number of extracted features was reduced using PCA, and a small number of features were selected to replace all the features, and a small number of features were not repeated.

Tumor classification

We used random forest for classification, which is an ensemble learning algorithm, and belongs to Bagging type. By combining multiple weak classifiers, the final result can be obtained by voting or taking the mean value, so that the result of the overall model can be characterized by relatively high accuracy and generalization performance. It can achieve good results, mainly due to "random" and "forest", one makes it have the ability to resist overfitting, the other makes it more accurate. The classification of tumor is performed by inputting the features of the segmented tumor into the classifier and training the classifier to output the classification results (benign or malignant). The data set comprised 274 images and the classifier adopts 5-fold cross-validation for training and testing. The results were expressed as the accuracy (the number of correct categories divided by the total number). For further evaluation, the sensitivity and specificity of classification were calculated. To ensure the integrity of the experiment, we compared the random forest classifier with the support vector machine, K adjacent separator and logistic regression classifier.

Observer study

Two radiologists with over 8 years of experience in breast MR imaging analyzed the images on the integrated computer workstation, without access to the final histological results. The diagnosis of the benign or malignant nature of the lesions was based on both the morphological characteristics and the time intensity curve (TIC) pattern of the lesions. First, Lesions were assigned to one of five categories

Table 1 Histological diagnoses of the examined benign and malignant breast lesions

Benign lesions ($n=154$)		Malignant lesions ($n=120$)	
Histopathologic diagnosis	n	Histopathologic diagnosis	n
Fibroadenoma	98	Invasive ductal carcinoma	96
Phyllodes tumor	32	Papillocarcinama	5
Papilloma	24	Invasive lobular carcinoma	16
		Paget's disease	3

as Score1 according to the Breast Imaging Reporting and Data System (BI-RADS) criteria (ACR 2013) by means of consensus by the two experienced radiologists after they analyzed the images without CAD. Second, the images were consecutively analyzed through CAD and the lesions were diagnosed as benign or malignant. Third, the two radiologists calculated Score 2 together with their final approval. Score 2 was calculated using rescaled CAD values added to the BI-RADS scores, according to the following equation: Score 2 = Score 1+CAD. The CAD was scored as − 1 when the CAD result was benign and as + 1 when the CAD result was malignant. Score 2 stands for the combined parameter BI-RADS and the CAD value. According to the BI-RADS system, the range of values were as follows: Category 1, negative findings; category 2, benign findings; category 3, probably benign findings; category 4, findings suspicious for malignancy; and category 5, findings highly suggestive of malignancy. The modified BI-RADS variable (score 2) was used only in the solid lesions. Therefore, score 2 should be between 3 and 5, and thus a value less than three was treated as 3; and that higher than five, as 5.

Pathological diagnoses

All breast lesions were confirmed histologically via surgery or biopsy. Lesions were first classified as malignant or benign, and then were divided into subgroups, as described in Table 1. All diagnoses were made by a pathologist with many years of experience in breast pathological examination.

Statistical analysis

The results of the analysis by the radiologists with and without CAD were evaluated using receiver operating characteristic (ROC) curve analysis. The BI-RADS results without CAD were established as Score 1 and the modified BI-RADS results that took into account the CAD results were established as Score 2. Score 2 was calculated together with the two radiologists' final approval.

The areas under the curve (AUC) were compared using a Hanley and McNeil test. Sensitivity and specificity values, and their respective 95% confidence intervals (CI), were estimated. A difference with a p value less than 0.05 was considered statistically significant. All data were analyzed using version 19.0 SPSS software (IBM Corp., Armonk, NY, USA).

Results

Breast MR imaging datasets and tumor segmentation

The 274 masses (mean size 27.8 ± 16.3 mm, range 8–63 mm) comprised 154 benign lesions and 120 malignant lesions. The histological diagnoses are shown in Table 1. The segmentation results obtained by preprocessing were compared with those obtained without preprocessing and are shown in Fig. 1.

Feature extraction

Fifty-one grayscale features and 15 gradient features of 274 images were generated using the GLCM and the GGCM. The 51 grayscale features were energy, correlation, contrast and homogeneity in three different relative distances (D = 1, 2, and 3), and four different relative angles (0, 45, 90, and 135 degrees) as well as mean, variance, and entropy. The 15 grayscale features were small gradient advantage, large gradient advantage, grayscale distribution inhomogeneity, gradient distribution inhomogeneity, energy, gray average, gradient average, gray mean–variance, gradient mean–variance, gradient entropy, correlation, gray entropy, entropy of mixing, inertia, and homogeneity. The contrast results for contrast, energy, consistency, and mean, extracted by the GLCM between the benign and malignant tumors, are shown in Fig. 2a. Extract the 13 shape characteristics of the image in the tumor: roundness, aspect ratio, average normalized radial length, normalized radial length standard deviation, entropy of the average normalized radial length, area ratio, aspect ratio, number of lobular, needle shape, boundary roughness, direction Angle, normalization of ellipse pupil ellipse normalized contour. The shape features are shown in Fig. 2b.

Classification results of CAD

In the 274 experimental images, there were 120 images with malignant tumors and 154 with benign tumors. Fifty-one grayscale features, 15 gradient features and 13 shape features of 274 images were generated. All 154 benign images were divided into five dissecting subsets, and the malignant data set was divided into five subsets. Each time, take one of the benign subsets and one of the malignant subsets as the test sets and the other four benign subsets and four malignant

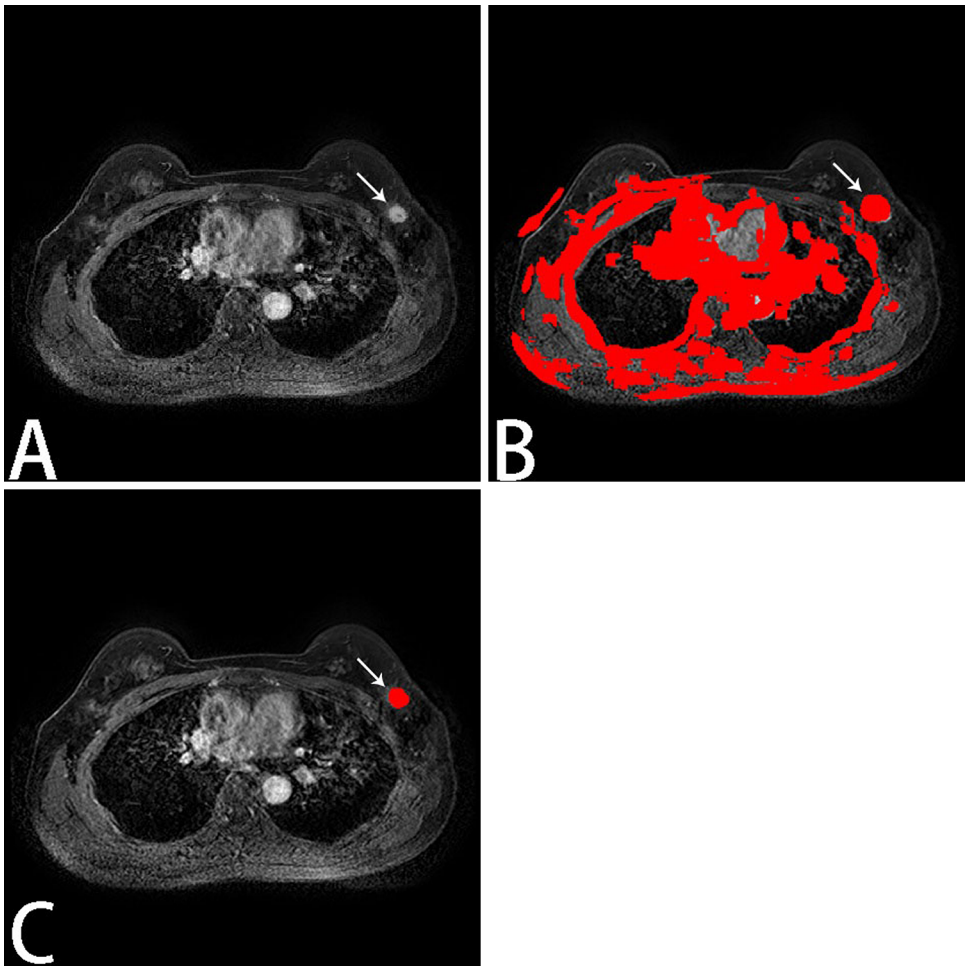

Fig. 1 Three cases for the segmentation results which were obtained by comparison. **a** The original image. **b** Image segmentation without preprocessing. **c** Image segmentation with preprocessing

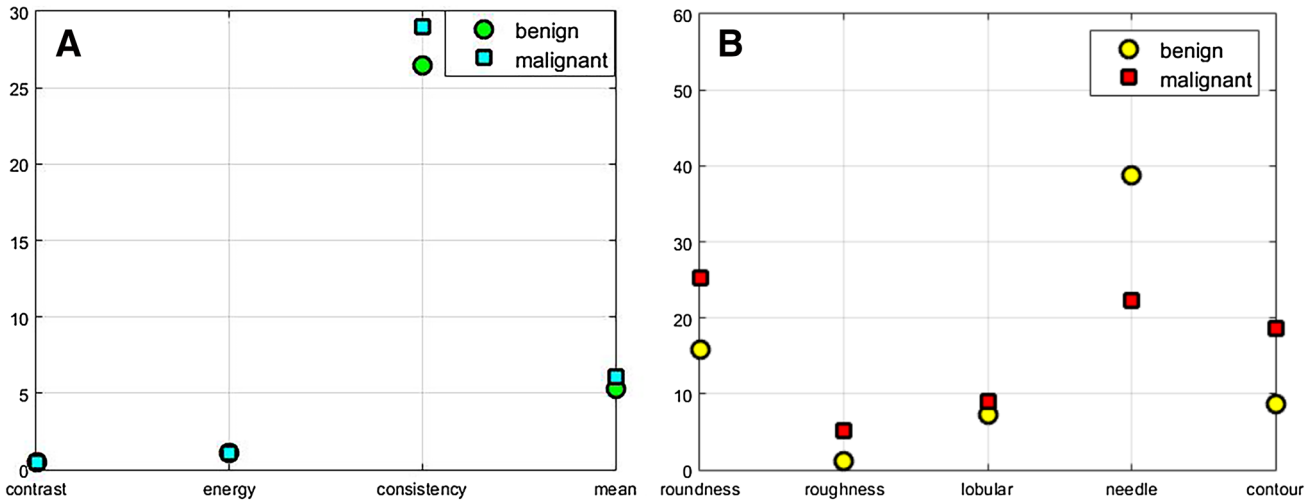

Fig. 2 Results of features contrast of the benign and malignant tumors, **a** the contrast results of the contrast, energy, consistency and mean extracted by the GLCM, **b** the contrast results of the roundness, roughness, lobular, needle, contour by the shape extraction algorithm

Table 2 The classification results of the four classifier

Classifier result	K adjacent	SVM	Logistic regression	Random forest
Accuracy	0.8704	0.9185	0.8852	0.9444
Specificity	0.9267	0.9067	0.8467	0.94
Sensibility	0.8	0.9333	0.9333	0.95

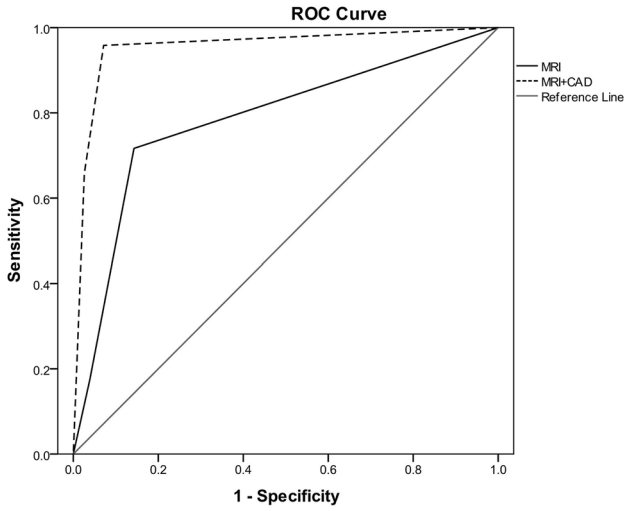

Fig. 3 Receiver operating characteristic (ROC) curves for score1 (BI-RADS) and score 2 (BI-RADS combined with CAD). The area under the ROC curve for score 2 was significantly higher than for score1

subsets as the training sets. Then, training the model or hypothesis function according to the training sets. Put this model on the test set and get the classification rate. Finally, we calculated the average classification rate obtained by five times as the real classification rate of the model or hypothesis function. We compared the random forest classifier with support vector machine (SVM), K adjacent separator and logistic regression classifier. The classification results are shown in Table 2. The results show that the random forest ensemble classifier (CAD) is superior to other classifiers, which achieved 94.44% accuracy, 95% sensitivity and 94% specificity.

Results of MR-CAD

The discriminating power to detect malignancy of variable score 2, with an AUC of 0.955 (95% CI 0.927–0.982) was significantly higher than that of score 1, with an AUC of 0.785 (95% CI 0.728–0.843; p, 0.0001; Fig. 3). The effect of the new variable (score 2) is shown in Table 3 and the greatest effect was observed in lesions of BI-RADS category 4 (n = 81). The original BI-RADS score of 4 was modified by addition of the CAD result to give a BI-RADS score of 3

Table 3 The BI-RADS categories for MR and MR-CAD

Categories	MR score1	MR-CAD score2
Category 3	166	148
Category 4	81	43
Category 5	27	83

for 16 lesions, and 65 cases were recategorized as BI-RADS 5. Cases with a BI-RADS score of 3 were modified to BI-RADS 4 for 34 lesions. Score 5 were modified to BI-RADS 4 for 9 lesions. The change to a score of BI-RADS 3 from BI-RADS 4 (16 cases) would have potentially avoided the need for biopsy, with these patients followed up for 6 months instead.

The sensitivity of score 2 was 95.8% and the specificity was 92.9%; whereas, the sensitivity and specificity of score 1 were 71.7% and 85.7%, respectively.

Discussion

In DCE-MRI, the breast lesions are mainly diagnosed based on morphological characteristics and the TIC curve patterns, according to the BI-RADS system. However, in this system, subjective factors might influence the categorization, and it is possible for different radiologists examining the same lesion to produce different categorizations.

The Gaussian mixture model algorithm has shown promising results in many different applications that contain image segmentation [14–17]; however, there have been few studies in breast tumor segmentation. In this study, we used a Gaussian mixture model and a random forest model for segmentation and classification. After segmentation, the tumors' morphological characteristics, such as the shape and the margins, were shown more clearly. The gray scale features, gradient features and shape features of the tumor were extracted and input into the random forest model for the classification of benign and malignant tumors. From the classification results, we observed that the random forest ensemble classifier is superior to other classifiers. The sensitivity and specificity were 95% and 94%, thus the CAD system has the potential to increase the reproducibility of the interpretation by radiologists in DCE-MR imaging and can benefit from differentiation among malignant and benign lesions, particularly when differences in computer-extractable information from DCE-MRI imaging reflect differences in tumor biological characteristics. Ming [18] trained a random forest using a leave one-out cross-validation (LOOCV) method to predict breast cancer subtypes. They fused the tumour- and parenchyma-based predictive

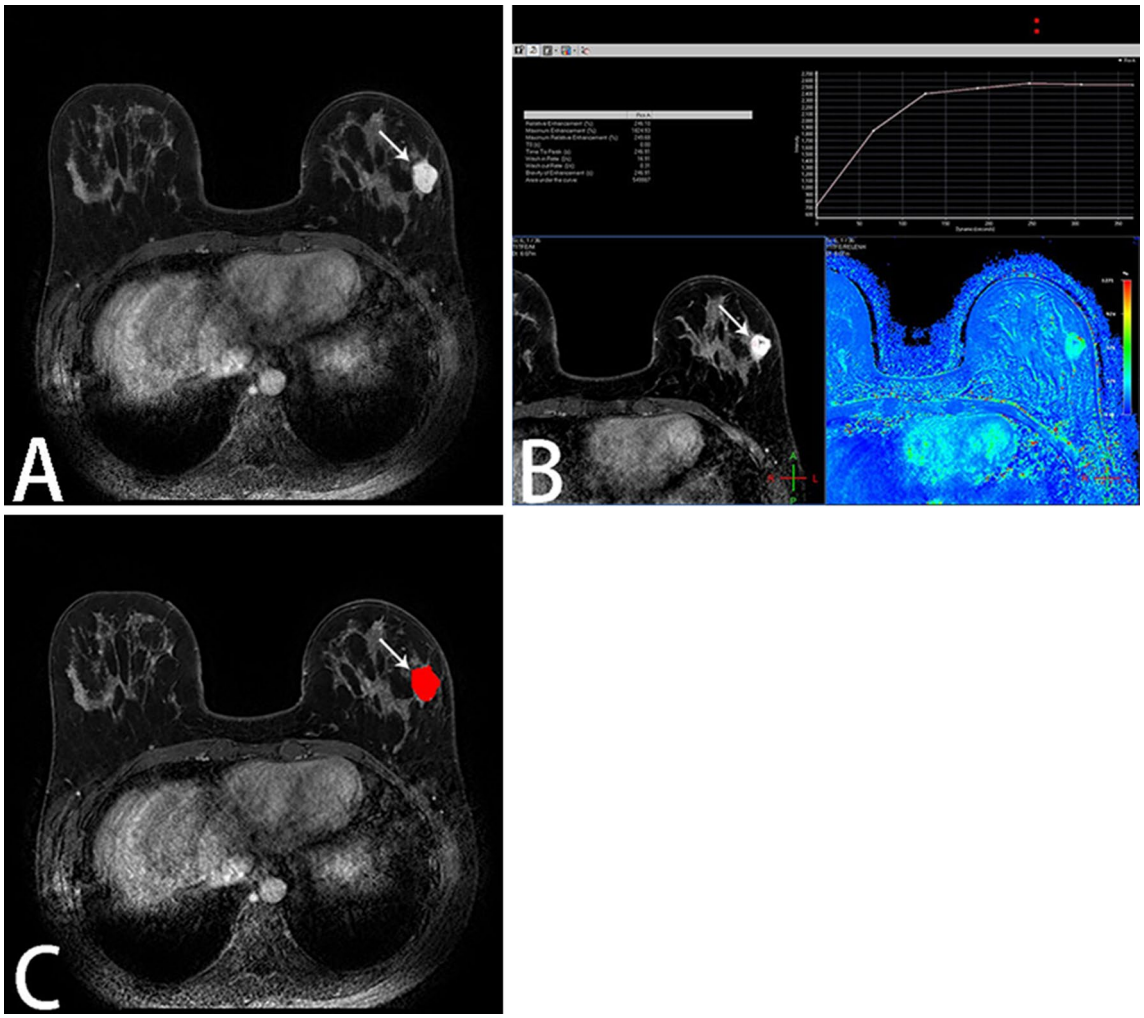

Fig. 4 Images obtained on examination of a 45-year-old woman with a solid lesion that was later confirmed histologically to be a fibroadenoma: **a** dynamic contrast-enhanced MR imaging, which depicts an non-homogeneous, solid lesion with irregular margins. **b** Time intensity curve (TIC) pattern is Type II. The lesion was classified as BI-RADS 4. **c** The lesion were segmented, the gray sale and gradient features were extracted, then the datas were inputed into the Random forest model for the classification, the result of CAD was benign, so the Score2=Score1 (BI-RADS 4)-1=BI-RADS 3

models of 211 samples, which finally achieved AUC of 0.897. Lindsay [19] extracted 230 features and put them into random forests, decision trees and logistic regression to train. Models were fit on 75% of the data and evaluated for probability calibration and area under the ROC curve (AUC) on the remaining test set and random forest method outperformed decision trees and logistic regression by an average AUC of 0.053 and 0.034, respectively. Huang [20] chose 3D morphologic features to perform the CAD progress, by using a training and validation set of 51 malignant and 44 benign lesions, achieved an AUC of 0.89 combing 3D morphologic and tumor shape features. However, only few studies evaluated breast lesions with radiologists' evaluations (BI-RADS).

Our results for the analysis by radiologists with and without CAD demonstrated that CAD is reproducible for MRI diagnosis. Variable score 2, which took into account both the BI-RADS categorization and the CAD values, ameliorated the overall diagnostic specificity (92.9% vs. 85.7%) and sensitivity (95.8% vs. 71.7%). The discriminating power to detect malignancy of variable score 2, with an AUC of 0.955 (95% CI 0.927–0.982) was significantly higher than that of score 1, with an AUC of 0.785 (95% CI 0.728–0.843; p, 0.0001; Fig. 3). In our study, the CAD modified the original BI-RADS scores of 4 to a score of 3 for 16 lesions (Fig. 4), which meant that biopsies could have been avoided in these cases. Therefore, we believe that CAD has the potential to assist in making the decision as to whether to perform percutaneous procedures, such as biopsy or fine needle aspiration (FNA). CAD may

be a valuable complementary method to differentiate benign from malignant breast lesions; however, larger clinical trials are required to validate our preliminary results.

There is an overlap in morphological characteristics between benign and malignant breast lesions; however, the benign and malignant lesions could be assessed on the same TIC (plateau curve). In our study, six benign lesions (three papilloma, two fibroadenoma, and one fibrocystic mastopathy) were mistakenly identified as malignant lesions by both the MRI and the CAD techniques. The TICs were all plateau curves and the morphological characteristics were also atypical, which may have interfered with the interpretation of the CAD results.

Our preliminary study had some limitations. First, our images were obtained from a single site, and almost all the malignant lesions included in our study were invasive ductal carcinoma. Therefore, additional studies with a greater variety of malignant and benign lesions in a larger series are required to establish the clinical value of CAD in the differential diagnosis of breast lesions. Second, no formal training for the processed images was used in our study. Although the features in the processed images were familiar to the radiologists, a training set to allow radiologists to become familiar with the CAD method might enhance their confidence to use it.

Conclusion

Our clinical investigation of 274 breast lesions showed that CAD is feasible to differentiate breast lesions, and can complement MRI, thereby making it easier to diagnose breast lesions and obviating the need for unnecessary biopsies. Further large prospective studies are required to fully determine the potential role of CAD.

Acknowledgements The study was supported by Postdoctoral Science Foundation of Ministry of Heilongjiang Province (Grant number LBH-Z17150).

Compliance with ethical standards

Conflict of interest None of the authors of this manuscript have a financial interest related to this work. Author's institutions have no conflicts of interest.

References

1. Mariscotti G, Houssami N, Durando M et al (2014) Accuracy of mammography, digital breast tomosynthesis, ultrasound and MR imaging in preoperative assessment of breast cancer. Anticancer Res 34:1219–1225
2. Lee-Felker SA, Tekchandani L, Thomas M et al (2017) Newly diagnosed breast cancer: comparison of contrast-enhanced spectral mammography and breast MR imaging in the evaluation of extent of disease. Radiology 285:389–400
3. Warner E, Plewes DB, Hill KA et al (2004) Surveillance of BRCA1 and BRCA2 mutation carriers with magnetic resonance imaging, ultrasound, mammography, and clinical breast examination. JAMA 292:1317–1325
4. Radhakrishna S, Agrwal S, Parikh PM et al (2018) Role of magnetic resonance imaging in breast cancer management. South Asian J Cancer 7:69–71
5. Roganovec D, Djilas D, Bujnovic S et al (2015) Breast MRI, digital mammography and breast tomosynthesis: comparison of three methods for early detection of breast cancer. Born J Basic Med Sci 15:64–68
6. Kanao S, Karaoka M, lima M et al (2018) Differentiating benign and malignant inflammatory breast lesions: value of T2 weighted and diffusion weighted MR images. Magn Reson Imaging 50:38–44
7. Jalalian A, Mashohor S, Mahmud R et al (2017) Foundation and methodologies in computer-aided diagnosis systems for breast cancer detection. EXCLI J 20:113–137
8. Honda E, Nakayama R, Toyama H et al (2016) Computer-aided diagnosis scheme for distinguishing between benign and malignant masses in breast DCE-MRI. J Digit Imaging 29:388–393
9. Song SE, Seo BK, Cho KR et al (2015) Computer-aided detection (CAD) system for breast MRI in assessment of local tumor extent, nodal status, and multifocality of invasive breast cancers: preliminary study. Cancer Imaging 8:1
10. Chaddad A, Luedi M, Zinn PO et al (2017) Corrigendum to "automated feature extraction in brain tumor by magnetic resonance imaging using gaussian mixture models". Int J Biomed Imaging 2017:1
11. Banaie M, Soltanian-Zadeh H, Saligheh-Rad HR et al (2018) Spatiotemporal features of DCE-MRI for breast cancer diagnosis. Comput Methods Progr Biomed 155:153–164
12. Gallego-Ortiz C, Martel AL (2016) Improving the accuracy of computer-aided diagnosis for breast MR imaging by differentiating between mass and non mass lesions. Radiology 278:679–688
13. Gubern-Merida A, Marti R, Melendez J et al (2015) Automated localization of breast cancer in dynamic contrast-enhanced-MRI. Med Image Anal 20:265–274
14. Spainhour JC, Janech MG, Schwacke JH et al (2014) The application of Gaussian mixture models for signal quantification in MALDI-TOF mass spectrometry of peptides. PLoS ONE 9:e111016
15. Gan H, Sang N, Huang R (2015) Manifold regularized semi-supervised gaussian mixture model. J Opt Soc Am A 32:566–575
16. Kawabata T (2018) Gaussian-input Gaussian mixture model for representing density maps and atomic models. J Struct Biol 203:1–16
17. Naidu BR, Babu MSP (2018) Biometric authentication data with three traits using compression technique, HOG, GMM and fusion technique. Data Brief 18:1976–1986
18. Fan Ming, Zhang Peng, Wang Yue et al (2019) Radiomic analysis of imaging heterogeneity in tumours and the surrounding parenchyma based on unsupervised decomposition of DCE-MRI for predicting molecular subtypes of breast cancer. Eur Radiol. https://doi.org/10.1007/s00330-018-5891-3
19. LindsayWD Ahern CA, Tobias JS et al (2018) Automated data extraction and ensemble methods for predictive modeling of breast cancer outcomes after radiation therapy. Med Phys 25:15. https://doi.org/10.1002/mp.13314
20. Huang YH, Chang YC, Huang CS et al (2013) Computer-aided diagnosis of mass-like lesion in breast MRI: differential analysis of the 3-D morphology between benign and malignant tumors. Comput Methods Progr Biomed 112:508–517